Ray-Tracing Evaluation of Diffuse Scattering in an Outdoor Scenario

Francesco Mani*, Claude Oestges†
ICTEAM - Electrical Engineering, Université catholique de Louvain
Louvain la Neuve, Belgium
*Francesco.Mani@uclouvain.be
†Claude.Oestges@uclouvain.be

***Abstract*—This paper compares radio channel measurements and ray tracing simulations in an outdoor environment. A model for diffuse scattering is implemented in a ay tracing tool. Simulations results show that this implementation is important to improve both pathloss and crosspolarization accuracy prediction. To improve delay spread prediction it is necessary to increase the maximum number of simulated interactions that a ray can undergo, at cost of a considerable increase of computation time.**

I. Introduction

Ray-tracing is a geometrical optics technique used to evaluate paths followed by rays as they interact with the environment. The starting point of this work is a classic 3-D ray-tracing (RT) software [1] that takes into account line of sight (LOS) propagation, specular reflection and diffraction. It has been already used in the past to predict wide and narrow band propagation characteristics in outdoor scenarios. The goal of this work is to enhance the prediction capabilities of the pre-existent tool. Diffuse scattering and penetration have been implemented for this purpose. This work follows a similar one previously done in an indoor scenario [2].

Although RT has been frequently used for outdoor propagation predictions (i.e. in [3], [4]), fewer results can be found on its usage to predict the polarization behavior of the channel [5], [6]. An accurate study on polarization characteristics of the channel is important for MIMO systems to exploit polarization diversity [7].

II. Diffuse Scattering Model

The model implemented into the RT tool is the one proposed in [8]. Diffuse scattring is supposed to model the interactions with rough surfaces, irregularities or small objects that can not be described in the input database of RT.

Each surface that experiences diffuse scattering is divided into surface elements. The size of each tile is set following the well known far-field condition [9]:

$$r > \frac{2D^2}{\lambda} \tag{1}$$

A diffuse scattering ray is supposed to originate from the center of each surface element. Diffuse scattering rays are assumed incoherent. For this reason they are added incoherently to the power given by LOS, reflections and diffractions. In this work diffuse scattering does not include any model for depolarization. This means that the same scattering coefficient is applied to both horizontal and vertical polarization components of the impinging wave.

Taking into account the results presented in [8], only a directive pattern model (Eq. 2) has been chosen for this outdoor scenario.

$$\left|\overline{E}_S\right|^2 = E_{S0}^2 \left(\frac{1+\cos\psi_r}{2}\right)^{\alpha_r} \tag{2}$$

The angle ψ_r is the one between the scattering and specular reflection direction. The parameter α_r sets the width of the scattering lobe: the higher the narrower the beam.

III. Measurements

The measurement campaign has been performed in a campus scenario in Louvain la Neuve, Belgium. The antennas used for the measurements were linear arrays of four dual-polarized ($+45°$ and $-45°$ slanted polarizations) patch antennas. Fig. 1 shows the map of the measurement scenario. The transmitter, in red in the picture, was placed on the fourth floor of a building, facing a pedestrian street. The receiver was moved in fifteen different positions along this street. Positions 1, 8, 9, 13, 14, 15 were in non-line of sight (NLOS) condition and in particular in positions 8 and 9, marked in white in the figure, the receiver was under a roof that was obstructing the LOS. Measurements were recorded with UCL-ULB Elektrobit MIMO Channel Sounder, which is based on a pseudo-random noise code technique. Its setup parameters for this campaign are shown in Table I.

In this scenario building façades are mainly made of brick while roofs are made of concrete. Table II shows the dielectric parameters of materials utilized in the simulations. For this work the presence of trees, that can be seen in Fig. 1, is not

TABLE I
Channel sounder setup parameters

Frequency	$3.8GHz$
Bandwidth	$200MHz$
Transmit Power	$23dBm$
Measurable Excess Delay	$10.23\mu s$
Time Resolution	$1.25ns$
Number of Channels	64
Cycles per Measurement	100

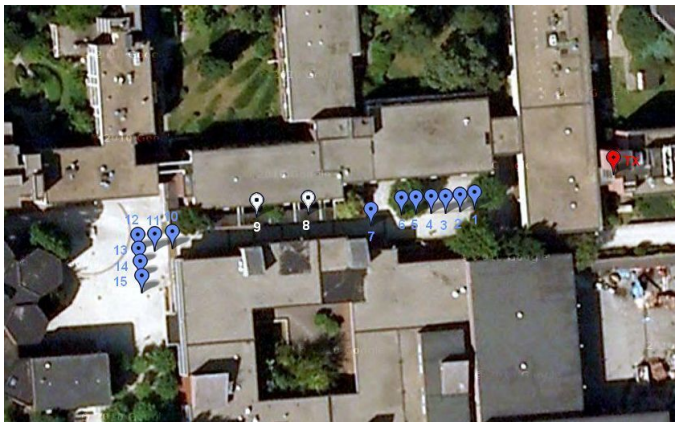

Fig. 1. Map of the measurement scenario

TABLE II
MATERIAL PROPERTIES AROUND $4GHz$

	ϵ_r	$\sigma[S/m]$
Brick	4.4	0.01
Concrete	8.5	0.2

taken into account in the simulations. However at the time of the campaign they were leafless.

IV. RAY TRACING SIMULATIONS

The outcome of the simulator is a discrete impulse response. To obtain a continous curve, it is convoluted with the normalized calibration impulse response that is chosen to represent the filter of the system. In addition to that, noise is removed from measurements applying a thresholding method. The threshold is set as the maximum value of the part of impulse response preceding the LOS, where it can be supposed there is only noise.

A sensitivity test with different values of scattering coefficient and different width of directive pattern model, set by parameter α_r, has been carried out. For this test, a maximum of three reflections has been used as well as single bounce scattering. The propagation parameter chosen to determine the best configugation is the pathloss. In this work, co-polar channels are the ones where antennas at both terminals have the same polarization, whereas cross-polar channels are those with orthogonal polarization at transmitter and reciever. Pathloss is evaluated taking into account co-polar channels only. Tables from III to VI show the results of this test. Fig. 2 shows the average prediction error for each parameter combination. Considering this outcome, in the following results, a directive model with $S = 0.3$ and $\alpha_r = 2$ has been utilized as it is the one that minimizes the prediction error.

Fig. 3 shows the pathloss comparison between measurements and simulations, when scattering is implemented or not in the simulator. From the graph it is possible to state that there is a general improvement after including diffuse component. As a matter of fact, the average prediction error drops from 10.1dB to 4.4dB. Excluding positions 14 and 15, that are deep NLOS, the improved tool shows good agreement

TABLE III
SENSITIVITY TEST ON PATHLOSS FOR $\alpha_r = 2$

	Measurements	$S = 0.2$	$S = 0.3$	$S = 0.4$
pos1	-89.1	-89.0	-85.9	-83.6
pos2	-83.6	-85.9	-84.0	-82.3
pos3	-80.4	-84.6	-82.9	-81.3
pos4	-78.8	-83.9	-82.2	-80.7
pos5	-80.3	-84.7	-82.7	-80.9
pos6	-82.3	-82.7	-81.4	-80.0
pos7	-83.2	-85.1	-83.1	-81.2
pos8	-91.1	-88.5	-85.4	-83.0
pos9	-96.7	-91.3	-87.7	-85.4
pos10	-89.9	-89.6	-89.2	-88.7
pos11	-93.6	-89.3	-89.9	-88.6
pos12	-90.2	-91.8	-91.4	-90.8
pos13	-94.8	-100.7	-97.9	-95.8
pos14	-95.5	-115.6	-112.4	-110.1
pos15	-104.4	-120.9	-117.3	-114.8

TABLE IV
SENSITIVITY TEST ON PATHLOSS FOR $\alpha_r = 3$

	Measurements	$S = 0.2$	$S = 0.3$	$S = 0.4$
pos1	-89.1	-88.4	-85.3	-82.9
pos2	-83.6	-85.6	-83.6	-81.8
pos3	-80.4	-84.3	-82.5	-80.9
pos4	-78.8	-83.6	-81.9	-80.3
pos5	-80.3	-84.4	-82.3	-80.4
pos6	-82.3	-82.5	-81.0	-79.6
pos7	-83.2	-84.7	-82.6	-80.7
pos8	-91.1	-87.8	-84.6	-82.2
pos9	-96.7	-90.5	-87.1	-84.6
pos10	-89.9	-89.5	-89.0	-88.5
pos11	-93.6	-89.2	-88.9	-88.4
pos12	-90.2	-91.5	-91.1	-90.5
pos13	-94.8	-99.9	-97.1	-94.8
pos14	-95.5	-115.1	-111.9	-109.5
pos15	-104.4	-120.7	-117.2	-114.7

TABLE V
SENSITIVITY TEST ON PATHLOSS FOR $\alpha_r = 4$

	Measurements	$S = 0.2$	$S = 0.3$	$S = 0.4$
pos1	-89.1	-87.9	-84.7	-82.4
pos2	-83.6	-85.4	-83.3	-81.4
pos3	-80.4	-84.1	-82.3	-80.5
pos4	-78.8	-83.5	-81.6	-80.0
pos5	-80.3	-84.2	-82.0	-80.1
pos6	-82.3	-82.4	-80.8	-79.3
pos7	-83.2	-83.5	-82.2	-80.3
pos8	-91.1	-87.3	-84.1	-81.7
pos9	-96.7	-90.0	-86.6	-84.1
pos10	-89.9	-89.4	-88.9	-88.2
pos11	-93.6	-89.2	-88.7	-88.2
pos12	-90.2	-91.6	-90.9	-90.2
pos13	-94.8	-99.3	-96.3	-94.0
pos14	-95.5	-115.8	-111.6	-109.3
pos15	-104.4	-120.8	-117.3	-114.8

TABLE VI
SENSITIVITY TEST ON PATHLOSS FOR $\alpha_r = 5$

	Measurements	$S = 0.2$	$S = 0.3$	$S = 0.4$
pos1	-89.1	-87.5	-84.3	-81.9
pos2	-83.6	-85.2	-83.0	-81.1
pos3	-80.4	-84.0	-82.1	-80.3
pos4	-78.8	-83.3	-81.5	-79.7
pos5	-80.3	-84.0	-81.8	-79.4
pos6	-82.3	-82.3	-80.6	-79.0
pos7	-83.2	-84.3	-81.9	-80.0
pos8	-91.1	-86.9	-83.7	-81.3
pos9	-96.7	-89.7	-86.2	-83.7
pos10	-89.9	-89.4	-88.8	-88.0
pos11	-93.6	-89.1	-88.6	-88.0
pos12	-90.2	-91.5	-90.8	-89.9
pos13	-94.8	-98.8	-95.7	-93.4
pos14	-95.5	-114.7	-111.5	-109.1
pos15	-104.4	-121.1	-117.6	-115.1

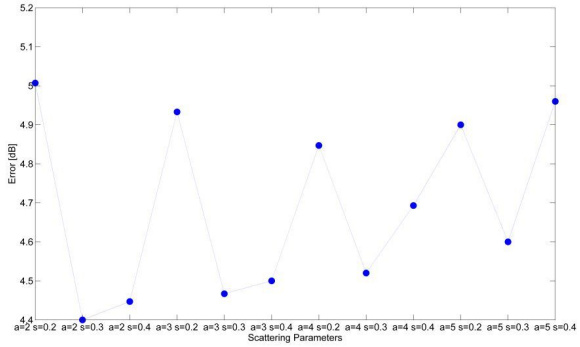

Fig. 2. Average pathloss error in dB for each scattering parameter combination

with measurements. The error taking into account only the first thirteen positions is 2.8dB.

In this paper, cross-polar discrimination (XPD) is defined as

$$XPD = 10 \log \left(\frac{P_{co}}{P_{xp}} \right) \tag{3}$$

where P_{xp} is the cross-polar power and P_{co} the co-polar power at the receiver. As previously done for pathloss, Fig. 4 is the

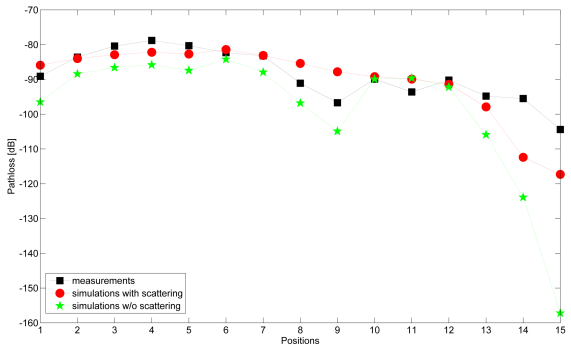

Fig. 3. Comparison of simulations with measurements for pathloss

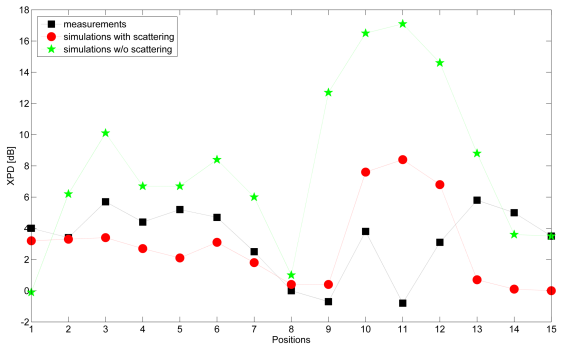

Fig. 4. Comparison of simulations with measurements for XPD

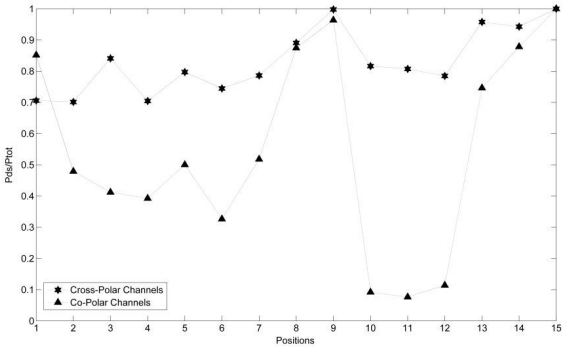

Fig. 5. Ratio between diffuse power and total received power for simulations

comparison between simulated and measured values of XPD. In this case the prediction error decreases from 5.5dB, when scattering is not included, to 2.8dB. It has to be noted that, while the tool without scattering seems to accurately predict the XPD in the two last measurement positions, these results are affected by the lack of accuracy of pathloss prediction. For example it will be shown that increasing the number of maximum reflections from three to four leads to a complete loss of accuracy in XPD prediction in position 15 if scattering is not included.

Fig. 5 shows the ratio between simulated diffuse power and simulated total received power, both for co-polar and cross-polar channels. It can be noted that, in the cross-polar channels, the power is for the greatest part composed by scattering, with an average ratio of 83%. In the co-polar channels the average ratio is 55%.

Some considerations can be made concerning the results presented. For example, taking into account that, for co-polar channels, it has been found that normally the percentage of scattering power in outdoor scenarios varies from 20% to 80% [10], the results presented in Fig. 5 shows that in NLOS conditions this percentage is generally exceeded. By contrast, in positions from 10 to 12, the level is lower than the expected one. In the same three positions, simulated XPD is higher than the measured one. This two results can be seen as a symptom of overestimation of the coherent component of the signal.

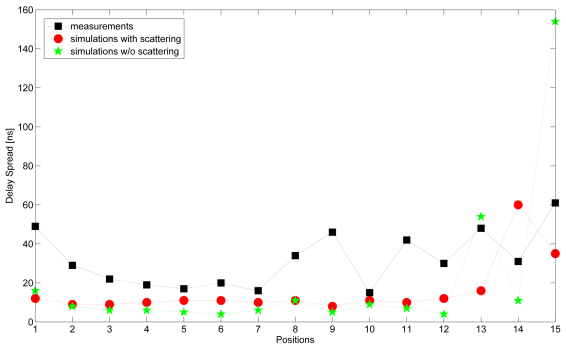

Fig. 6. Comparison of simulations with measurements for delay spread

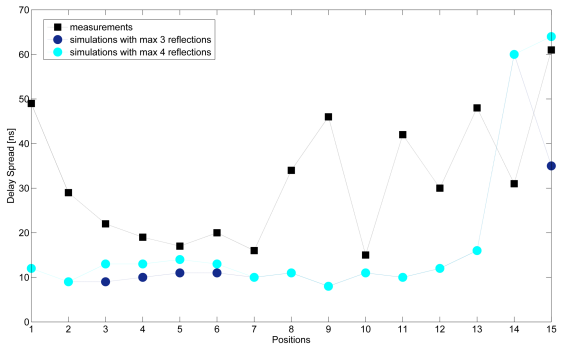

Fig. 7. Comparison of delay spread results for simulations with scattering with different levels of maximum possible reflections

This might be due to the fact that the presence of trees was not taken into account in the simulations. Something can also be said about NLOS positions from 13 to 15, where the XPD prediction underestimates the measurements. Considering that in positions 14 and 15 pathloss is also significantly underestimated, it could mean that there is some coherent path that is not estimated by the tool. On the other hand, in position 13 pathloss prediction is good. So an alternative conclusion could be that there is need of a better modelization of polarization behavior of scattering, which is the most significant part of the power received in NLOS conditions.

Delay spread is defined as:

$$t_{ds} = \sqrt{\frac{\sum_i \left(t_i - \frac{\sum_i t_i P_i}{\sum_i P_i}\right)^2 P_i}{\sum_i P_i}} \qquad (4)$$

where t_i is the time of arrival and P_i is the power of the i^{th} contribution. Fig. 6 shows the comparison between simulated, with and without scattering, and measured delay spread. While the results show a slight improvement after the implementation of scattering, there is a significant underestimation of the measurements.

The number of maximum reflections that a single ray can experience has been increased from three to four. This does not affect the prediction error of the simulations with scattering for pathloss and XPD. On the other hand, it affects prediction error in position 15 in the simulations without scattering. It decreases the error for pathloss but it increases significantly the one for XPD, confirming the assumption that the good match with the measurements was not trustable in that case. The average prediction error, in the simulations without scattering, becomes 8.6dB for pathloss and 6.4dB for XPD. Fig. 7 shows that delay spread prediction, instread, is improved, even if just in some positions.

Finally, scattering interaction followed or preceded by a single reflection as been added to simulations. Considering also four maximum reflections, the prediction error for pathloss decreases from 4.4dB to 3.5dB. This is due to an significant improvement in prediction for the last three positions (deep NLOS). Concerning XPD, the prediction error decreases from

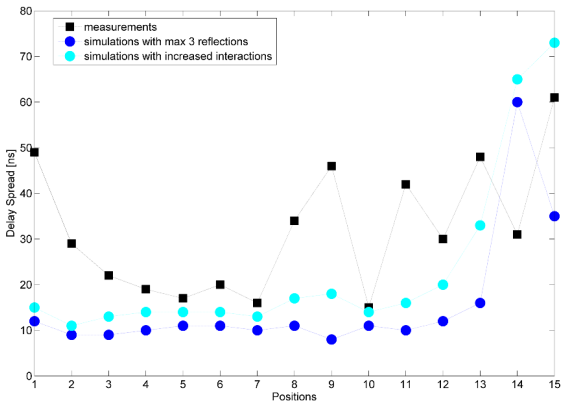

Fig. 8. Delay spread results for simulations with four maximum possible reflections and scattering with a reflection before or after

from 2.8dB to 2.6dB. Fig. 8 shows that in this case delay spread prediction is generally improved, but the underestimation is always present.

V. Conclusions

This paper has presented measurements and simulations in an outdoor campus scenario. A diffuse scattering model has been implemented within a RT tool. Results of simulations for pathloss, XDP and delay spread are presented and compared with measurements. The sensitivity of pathloss has been tested with respect to diffuse scattering parameters.

The results presented in this paper shows that diffuse scattering is important to obtain accuracy of pathloss and XPD prediction even in outdoor scenario. The improvement is significant and the simulations generally show good agreement with measuremtnts. Considering delay spread, diffuse scattering improves the accuracy of prediction marginally. A more perceptible improvement is noted if the number of interactions allowed for each ray is increased, but this costs significantly in terms of computation time. In any case, there is a general underestimation of measured delay spreads.

The study of the impact of propagation loss and scattering by trees and the study of polarization behavior of diffuse

scattering can be foreseen as future work to improve even more the simulation accuracy.

ACKNOWLEDGMENT

The authors would like to thank Pat Chambers and Nizabat Khan (ICTEAM - Electrical Engineering, UCLouvain) for their help in conducting the measurement campaign and Vittorio Degli Esposti and Enrico Maria Vitucci (DEIS, University of Bologna) for their significant input to the implementation of diffuse scattering model.

This work was supported by Région Wallone in the framework of contract 616417 BIRADAR and of contract C-6321 S@T, by the European Commission in the framework of the FP7 Network of Excellence in Wireless COMmunications NEWCOM++ (contract no. 216715) and the COST 2100 Action. Claude Oestges is pleased to acknowledge the financial support of the Belgian Fonds de la Recherche Scientifique.

REFERENCES

[1] C. Oestges, B. Clerckx, L. Raynaud, and D. Vanhoenacker-Janvier, "Deterministic channel modeling and performance simulation of micro-cellular wide-band communication systems," *IEEE Trans. Veh. Technol.*, vol. 51, no. 6, pp. 1422–1430, November 2002.

[2] F. Mani and C. Oestges, "Evaluation of diffuse scattering contribution for delay spread and crosspolarization ratio prediction in an indoor scenario," in *4th European Conference on Antennas and Propagation - EuCAP*, Barcelona, Spain, April, 12-16 2010.

[3] T. Fügen, S. Knörzer, M. Landmann, R. Thomä, and W. Wiesbeck, "A 3d ray tracing model for macrocell urban environments and its verification wih measurements," in *2nd European Conference on Antennas and Propagation - EuCAP*, Edinburgh, Scotland, Nov. 2007.

[4] K. H. Ng, E. K. Tameh, A. Doufexi, M. Hunukumbure, and A. R. Nix, "Efficient multielement ray tracing with site-specific comparisons using measured mimo channel data," *Vehicular Technology, IEEE Transactions on*, vol. 56, no. 3, pp. 1019 –1032, may. 2007.

[5] G. Yang, K. Pahlavan, J. Lee, A. Dagen, and J. Vancraeynest, "Prediction of radio wave propagation in four blocks of new york city using 3d ray tracing," in *Personal, Indoor and Mobile Radio Communications 1994, 5th IEEE International Symposium on*, vol. 1, sep. 1994, pp. 263 –267 vol.1.

[6] V. DegliEsposti, V. Kolmonen, E. Vitucci, F. Fuschini, and P. Vainikainen, "Analysis and ray tracing modelling of co- and cross-polarization propagation in urban environment," in *2nd European Conference on Antennas and Propagation - EuCAP*, Edinburgh, Scotland, Nov. 2007.

[7] W. Lee and Y. Yeh, "Polarization diversity system for mobile radio," *Communications, IEEE Transactions on*, vol. 20, no. 5, pp. 912 – 923, oct. 1972.

[8] V. DegliEsposti, F. Fuschini, E. M. Vitucci, and G. Falciasecca, "Measurement and modelling of scattering from buildings," *IEEE Trans. Antennas Propagat.*, vol. 55, no. 1, pp. 143–154, January 2007.

[9] ——, "Speed-up techniques for ray tracing field prediction models," *IEEE Trans. Antennas Propagat.*, vol. 57, no. 5, pp. 1469 – 1480, May 2009.

[10] J. Salmi, J. Poutanen, K. Haneda, A. Richter, V.-M. Kolmonen, P. Vainikainen, and A. F. Molisch, "Incorporating diffuse scattering in geometry-based stochastic mimo channel models," in *Antennas and Propagation (EuCAP), 2010 Proceedings of the Fourth European Conference on*, 2010, pp. 1 –5.